THE RIGAKU JOURNAL
VOL. 21 / NO. 1 / 2004, 2–14

STRUCTURE DETERMINATION FROM POWDER DIFFRACTION DATA–CHALLENGING BATTERY MATERIALS

PETER Y. ZAVALIJ AND M. STANLEY WHITTINGHAM

Department of Chemistry and Institute for Materials Research, State University of New York at Binghamton, Binghamton, NY 13902, USA

In recent years, the search for novel and improving existing materials that can be used as a cathode in rechargeable lithium batteries become one of the most important priorities of modern technology. This work discusses some structural features and transformation of the battery related materials. It summarizes peculiarities and additional challenges imposed by the open frameworks on powder structure determination, which is already far from trivial. Despite the difficulties, *ab-initio* crystal structure solution was successfully used to determine the structure of nearly 20 battery related materials. Most of the structures were challenging in many different ways: *ab-initio* indexing in the presence of other phases or pseudo-symmetry; powder pattern decomposition and Rietveld refinement with substantial peak broadening or overlapping; complex preferred orientation and its handling during the structure solving and refinement. The main challenge–solving the structure was done using either the reciprocal space approaches such as heavy atom (Patterson) method and direct methods, or the real space modeling such as geometry optimization, energy minimization, and global optimization, but always involving de facto or a priori chemical and structural knowledge as well as any available analytical data.

1. Introduction

Open framework materials play an important role in heterogeneous catalysis, rechargeable batteries, ion exchange, molecular sieves, and other applications where multiple cycles of intercalation/deintercalation are of main concern [1]. Demand on novel or improved existing materials for rechargeable lithium batteries is growing in accord with rapid development of modern technology, mostly because of the need of advanced energy sources for various electronic devices starting from miniature but long lasting medical pumps or monitors, e.g. heart support, to large and powerful batteries for hybrid electric vehicles. Such a broad spectrum of battery applications implies a wide range of their properties. The most important of which are the capacity either by weight or by volume, the lifetime of the battery, as well as its safety and environmental issues.

In order to improve existing or develop novel materials, establish structure–property relationship, and find more effective synthetic routes, the knowledge of the crystal structure and understanding the structural changes during the battery performance is one of the first priorities. Thus, the structure has to be determined using either the single crystal or the powder diffraction methods. The former one is limited by the size and the quality of the crystals obtained during the synthesis. This seldom can be improved by re-crystallization not only because of the extended framework but often because of the metastable nature of the hydrothermally prepared phases. Moreover, intermediate substances or materials that undergo multiple intercalation/deintercalation cycles rarely form single crystals of suitable size and often have low crystallinity or even become amorphous. Despite the substantially lowered requirements in the size of the single crystal due to the use of the area detectors, the crystal must still be several teens of microns at the best. Thus, in many cases the structural studies must be conducted using the powder diffraction data, which have been substantially improved during the last decade mainly because of the development of new methods and software but also due to much faster computing.

2. Battery Materials

The operation of rechargeable lithium batteries is based on the intercalation/deintercalation of the lithium ions. The battery consists of a cathode, anode and electrolyte as shown in Figure 1 (top). The cathode today is made of a transition metal oxide or phosphate with the open framework structure with additions of binder

(Teflon) and conductor (acetylene black). The anode is typically pure lithium, lithium intercalated graphite or a lithium alloy. The electrolyte is an organic solvent with added lithium salt to allow the transport of lithium ions between the two electrodes. A separator, which is wetted by the electrolyte system, prevents electronic shorting so that only lithium ions can move back and forth. When the battery is discharging, the Li ions move through the electrolyte towards the cathode and intercalates into the open structure material. The electrons move towards the cathode though the load (upper half of the circuit) and are absorbed by the transition metal oxide or phosphate framework. The transition metal is being reduced decreasing its oxidation state. When the battery is charged, all processes are reversed; the electrons, the Li ions, and the current flow in the opposite direction and transition metal is being oxidized. All that demands certain specific requirements of the cathode material. It should be able intercalate and deintercalate lithium without substantial structural changes in the open framework.

The structure transformation can also take place but both structures should be closely related and be able to transform one into another without or with only minimal changes in the connectivity or bonding. On the other hand the charging/discharging of the battery being a redox reaction requires the framework metal to have more or less wide range of oxidation states, for which the metal coordination polyhedra are similar, if not the same. For example, vanadium in the oxidation states 2+ and 3+ has a regular octahedral environment, while for vanadium 5+ and 4+ the octahedra are distorted and may even become square pyramid (one corner missing). Thus, vanadium compounds can theoretically cycle up to 3 Li atoms per one V atom.

Typical cycling of the battery material shown in Figure 1 (bottom) reveals the properties of the electrochemical cell, of which the capacity and capacity fading are of main concern. The former shows the total charge that can be accumulated in the battery, while the latter—capacity fading (or cyclability) defines the battery lifetime. Potential of the cycle depends on the type of the battery material and is of less importance. For example, when it is low (e.g. below 1 V) the material can be potentially used not as the cathode but as the anode material. In order to be considered for commercial use, the battery materials should have capacity of at least 120 mAh/g and good cyclability—show no substantial loss of the capacity for hundreds of cycles. The safety and environmental issues are also of great concern.

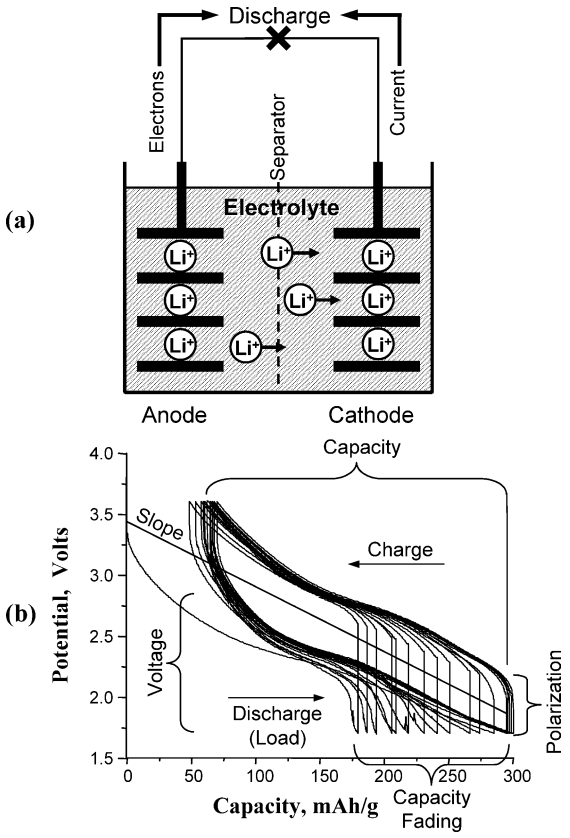

Fig. 1. The scheme of the lithium battery on discharge, when charging the direction of all arrows alternates (top), and the electrochemical cycling diagram showing most important battery parameters (bottom).

Based on the structural transformation during the cycling, the electrochemical cells are divided into two types. The first, shown in Figure 2, a, is so called single phase or solid solution. In this case the battery material always consists of single phase, which composition (the lithium content) changes continuously in the course of the intercalation/deintercalation process. The second type, shown in Figure 2, b, is two phase system. Here no solid solution is formed. During the intercalation/deintercalation reaction the ratio between the two phases changes but the content of the lithium in each phase is constant, so the cell voltage remains constant.

Often a complex combination of one or both of the two cases is observed as shown in Figure 3 for the reaction of lithium into metallic tin foil that was tested for anode material [2]. Here during the electrochemical discharge the following phase transitions occurs:

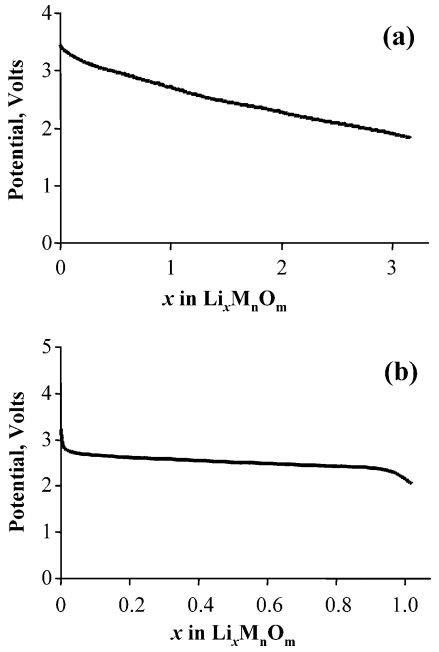

Fig. 2. Discharge semi-cycle in: a) solid solution system always consisting of one phase with variable content of the lithium $Li_xM_nO_m$ ($x \geq 0$) ; b) two phase system in which the Li content is defined by ratio between two phases $xLiM_nO_m+(1-x)M_nO_m$ ($0 \leq x \leq 1$) (the caption shows the total composition of the sample).

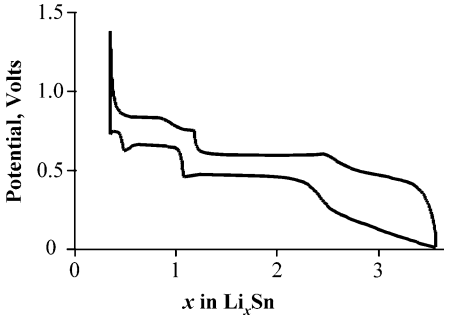

Fig. 3. Electrochemical cycling in a complex multistep system Sn–Li3.5Sn.

$$Sn \rightarrow Li_{0.4}Sn \rightarrow LiSn \rightarrow Li_{2.3}Sn$$
$$\rightarrow Li_{2.6}Sn \rightarrow Li_{3.6}Sn.$$

These phase changes combined with the structural and chemical requirements for the open framework materials discussed previously make the powder diffraction method an effective and often irreplaceable tool for studying open frameworks of battery materials. For example, accurate unit cell refinement in the solid solution systems or the Rietveld structure refinement in two-phase system can be used to determine Li content in the process of the charge/discharge process. This is especially useful when in situ diffraction is used. Of course, the crystal structure solution of novel compounds and accurate structure refinement of known or improved materials are essential in establishing the structure—property relationship. There is only one example when single crystal analysis was used, which is the study of $Li_nV_6O_{13}$ system using special electrochemical cell to grow lithiated crystals [3–5]. The current state of the powder structure determination leaves no excuses when such valuable information is omitted from the materials characterization.

3. Powder Structure Determination

The diffraction pattern from polycrystalline materials can be described as one-dimensional projection of three-dimensional diffraction data that results partial and/or complete overlapping of some diffraction maxima (peaks). The overlapping defines the principal difference between the powder and single crystal diffraction patterns and makes the former more challenging. However, the main challenge is not in the powder structure determination itself but in doing it from the diffraction data which quality or crystallinity is not the best. The reason for this is that the good crystallinity means quite high chance of finding a crystal suitable for single crystal experiment. However, when dealing with crystalline materials of low quality or crystallinity, those that exhibit low diffraction intensity or broad peaks, the single crystal diffraction usually fails, while the powder method still can yield acceptable patterns. From another point of view, the preference or necessity of the powder diffraction consists in inability to grow suitable crystals because of the metastability of many of the open framework materials or because of limits imposed by the synthetic routes used. The powder diffraction is also irreplaceable for *in situ* studies. It is the only way to determine or confirm the structure of the resulting and intermediate phases and their transition in the intercalation/deintercalation process. Examples of typical polycrystalline materials are shown in Figure 4, none of those crystals have size and quality acceptable for the routine single crystal experiment.

The three main steps in the powder structure determination, not counting instrumental and sample preparation issues, are following:

– indexing the powder pattern (determination of the unit cell dimensions);
– solving the crystal structure of new materials;
– the crystal structure refinement and complet-

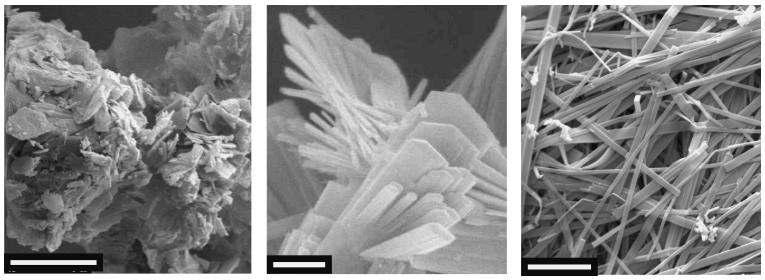

Fig. 4. SEM images of $VO(OCH_2CH_2O)$ [6], γ-MnV_2O_5 [7], and $tmaV_8O_{20}$ [8]. White bar corresponds to 10 μm.

ing the structural model.

Indexing the powder pattern

The first step consists in finding the unit cell dimensions that best describe the position of the diffraction peaks on the powder pattern. No mistakes are tolerated at this stage because failure or incorrect solution disables the following structure determination.

The indexing can be performed using variety of the available methods such as already classic program ITO [9], TREOR [10] and DICVOL [11] that use position of the diffraction peaks and recently developed algorithms realized, for example, in McMaille [12] and Xcell [13] that employ global optimization and global search of the unit cell dimensions. All software generate several best possible solutions and the role of the investigator, which is still very important, is to decide which solution is the true one or at least which one to start test with. Obviously, the final proof of the unit cell correctness is the determination of the crystal structure.

The main challenges in the pattern indexing that has to be considered are:

- systematic error in the peak positions because of sample transparency of samples with medium to low absorption and other effects;
- presence of impurity peaks;
- accidental non-crystallographic relationship between the cell dimensions;
- factors decreasing accuracy in the peak positions such as peaks overlapping and broadening.

In case of the open framework materials in addition to the general problems listed above the following issues have to be considered:

- additional weak diffraction peaks from the sublattice or modulated lattice, which sometimes happen in case of misfit—the size of intercalated species does not match the periodicity of the framework;
- substantially intensified peaks for the reflections from only one zone due to the significant preferred orientation effect that cannot be predicted at this stage;
- high anisotropy of the peak broadening and others.

Solving the crystal structure

Obviously, this step is the most important in the structure determination and consists in creation of the structure model as close to global minimum (true structure) as possible. Sometimes the model can be imported from similar or isostructural phases or derived from general crystal-chemical considerations for relatively simple compounds. Usually the structure of novel material has to be solved from the first principals. There are two principally different approaches of doing that:

- The first, traditional approach works in the reciprocal space (diffraction data) using direct methods or heavy atom (Patterson) method. It requires preliminary determination of the diffraction intensity of the individual reflections (as accurate as possible), which is done using profile fitting or full pattern decomposition methods [14, 15]. The real space (the structure itself) is used to evaluate the reasonability of a generated model. Basically the same programs that are used to solve single crystal structures are used to solve structure from the powder diffraction data, e.g. SHELXS [16].
- The second approach searches for a model in direct (or real) space and evaluates the quality of the model by comparing calculated profile to the experimental diffraction pattern. Most commonly used programs for *ab initio* structure determination exploit variety of global optimization methods, for example simulated annealing or parallel tem-

pering algorithms realized in FOX [17] and PowderSolve [13].

It is up to the researcher to decide which model is true, if several close solutions are found, and check its common chemical and crystal-chemical sense. The final structure is always confirmed by the following Rietveld refinement.

The main concern in solving the structure from the powder data is resolution of the reflections on the diffraction pattern. Any substantial overlapping of the reflections lowers the quality and makes the true solution less distinguishable. Heavy overlapping makes the structure determination very difficult if not impossible. In this case the direct space search, e.g. global optimization method, becomes much more advantageous. Additional difficulties in the powder structure solution, that are usually found when dealing with the open framework materials, are provided by factors that affect intensity of the diffracted peaks, for example such as huge preferred orientation or weak absorption, and other factors that decrease intensity or increase broadening of the peaks.

Crystal structure refinement—the Rietveld method

The refinement of the crystal structure from powder diffraction data is conducted by the Rietveld refinement [18] that employs least-square method to minimize the difference between observed and calculated powder patterns. This implies that in addition to the atomic parameters, which are the only parameters optimized in the single crystal refinement, there are parameters that describes the profile of the powder diffraction pattern and some other corrections. These are:

- cell dimensions which define the position of the peaks;
- parameters describing shape of the diffraction peaks and its angular distribution;
- parameters, such as preferred orientation and absorption, that affect the diffracted intensity.

The preferred orientation and absorption corrections are very important in the powder structure refinement in general and are of the special concern when dealing with the open framework materials that are often layered materials. The preferred orientation effect results in non-random orientation of the particles that depends on their shape. The two common shapes are plates and needles or fibers, examples of which are shown in Figure 4, b, c respectively. Obviously, it is almost impossible to achieve completely random distribution of the particles with such anisotropic shape. Especially in such case as one depicted in Figure 4, c. The distribution of these ribbon-like crystals is highly anisotropic and therefore very complicated and its proper handling requires two axes for the classic March–Dollase preferred orientation function [19] or complex distribution function, e.g. such as realized in spherical harmonic approach [20].

There is variety of the software for the Rietveld refinement: freeware GSAS [21], Rietica [22], FullProf [23], along with commercial Reflex [13], WinCSD [24], and many other.

Detailed discussion on powder diffraction methods and structure determination from powder data is discussed in many books, from which the most recently published [25–28] cover X-ray powder diffractometery, the Rietveld refinement, modern methods of the structure solution, and other aspects.

4. Structure Determination of Battery Materials and Related Compounds

The search for new battery materials and improvement of the existing ones has been conducted at the Institute for Materials Research at Binghamton University for more than decade [29]. The crystal structure of several dozens of the novel compounds was determined from the powder diffraction data. Obtained structural information in combination with single crystal results was used: to analyze the relationship between different structure types, e.g. in vanadium oxide frameworks [30]; to establish structural changes or phase transition during the intercalation and deintercalation processes in the electrochemical cell, e.g. in Li–$VOPO_4$ systems [31]; to improve synthetic methods, e.g. role of the pH in synthesis of the vanadium oxide frameworks [32, 33]; or to link the red-ox properties with the coordination of the transition metal [30].

This work summarizes and discusses the powder structure determination issues for these materials and some of their structural features.

4.1. Layered Molybdenum Oxide Structures

The use of molybdenum compounds as the battery materials is limited by their weight capacity that is low comparing to 3 d metal oxides. However, molybdenum exhibit wide range of the oxidation states and readily form the open framework structures. Because of that the molybdenum compounds can be used as model materials. The cluster or ionic molybdenum compounds crystallize very well but the open

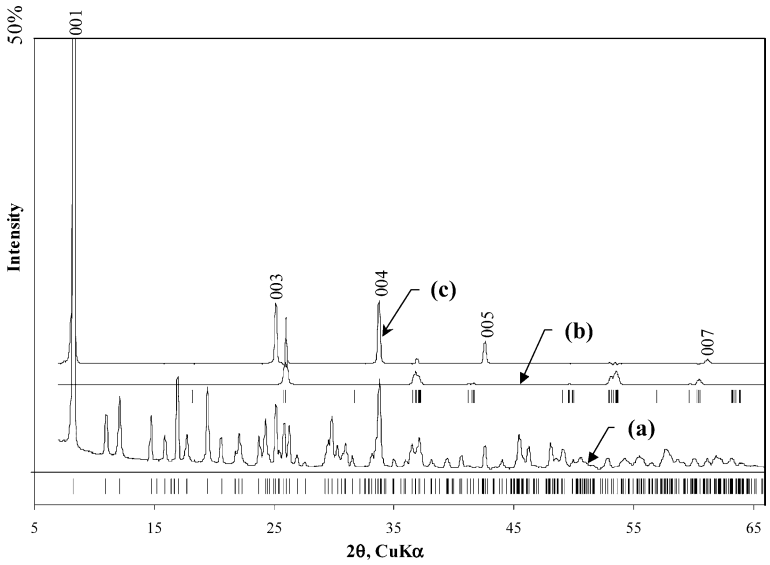

Fig. 5. The Rietveld refinement of $tmaMo_4O_{12}$: a) the observed plot with subtracted (b) and (c); b) calculated plot for MoO_2 phase; c) calculated plot for a thin surface layer of the main phase. The vertical lines show the position of the reflections.

framework materials, especially layered ones often produce only polycrystalline samples. For example the tetramethylammonium (tma) and methylammonium (ma) form at hydrothermal conditions fine powders, which crystal structure was determined from the powder diffraction data as is discussed below.

$tmaMo_4O_{12}$ [34]

Tetramethylammonium, $[N(CH_3)_4]^+$, intercalates into molybdenum oxide to form fine bronze powder. The powder pattern was indexed in a monoclinic system and crystal structure solved by direct methods using extracted integrated intensities. Two independent Mo atoms found initially were enough to locate 9 light atoms (except hydrogen) from the consequential difference Fourier maps. The position of remaining two carbon atoms was calculated from geometrical considerations. This material exhibits strong and unusual preferred orientation because of graphite-like morphology of the particles. It consists of three "phases", which profiles are shown separately in Figure 5:

a) the main $tmaMo_4O_{12}$ phase with March–Dollase PO refined to give a reasonable magnitude* of about 1.5;
b) an impurity phase that was identified and refined as MoO_2;
c) a thin surface layer of practically parallel platelike particles of the $tmaMo_4O_{12}$ phase that approximately doubles intensity of the *00l* reflections, for which an additional scale multiplier was introduced†.

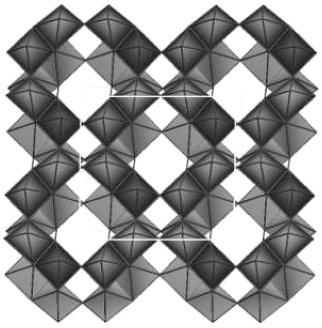

Fig. 6. Polyhedral representation of the Mo_4O_{12} layer.

The final Rietveld refinement (sp. gr. C2/m, $V=1434.9(3)$ Å^3, $2\theta_{max}=66°$, 287 reflections, 13 independent atoms, $R_B=9.6\%$, $R_p=10.4\%$, PO axis 001, total magnitude 3.5) was conducted without any constraints. Despite the strong PO, complex structure and somehow broad peaks, especially at higher angles, refinement resulted in good agreement between observed and calculated profiles, reasonable coordination polyhedra, bond lengths, and intermolecular contacts. Practically identical layer (Figure 6) was found later in $enH_2Mo_4O_{12}$ structure solved from single crystal data [35].

$ma_2Mo_7O_{22}$ [36]

This molybdate has more complex structure.

* Ratio of the maximal to minimal PO corrections.

† Sample was never pressed but surface had to be flattened with razor. Using the side filling or mixture with amorphous substance resulted no improvement on the particle distribution.

The powder pattern was indexed in a monoclinic system using ITO program. Initial model of the Mo_7O_{22} layers was incorporated from known thallium structure [37], which was found using exact composition determined thermogravimetrically. The intercalated methylammonium ion, $[CH_3NH_3]^+$, was undoubtedly located from the difference Fourier map. Contact distances to oxygen atoms were used determine the orientation of the ma cation, based on the hydrogen bonds formed. The Rietveld refinement (sp. gr. C2/c, V=2092.22(4) Å^3, $2\theta_{max}$=98°, R_B=3.8%, R_p=4.7%, PO: March–Dollase, axis 100, magnitude 2.2) converged without any constraints at low residuals despite the complexity of the structure (17 independent atoms) and the diffraction pattern (1026 reflections).

4.2. Simple Vanadium Oxides

Vanadium oxide structures were found to form even broader diversity of the open frameworks than molybdenum compounds, which along with wide range of the oxidation state and light weight, make them very promising battery cathode materials. The series of novel vanadium oxides and intercalates were prepared using hydrothermal technique. Many of these novel materials can be obtained only in polycrystalline from and, therefore, the powder diffraction data have to be exploited to determine their crystal structure that is discussed further.

$Li_xV_{2-\delta}O_{4-\delta}\cdot nH_2O$ [38]

This simple structure with just several diffraction peaks on the powder pattern, which was indexed using TREOR program in a tetragonal body-centered cell. Analysis of the Patterson map resulted positions of one vanadium and two oxygen atoms. Further refinement revealed the presence of the water molecule between the layers. However, there were some complications: noticeable higher displacement parameters for the heavier vanadium atoms comparing to the lighter oxygen atoms of the framework, and water molecule residing on the fourfold axis appeared to have a disk-like ellipsoid.

The final Rietveld refinement (sp. gr. I4/mmm, V=216.95(2) Å^3, $2\theta_{max}$=100°, 42 reflection, 4 atoms, R_B=4.0%, R_p=8.3%, PO: WinCSD, axis 001, magnitude 1.2) included an occupation factor of the vanadium atom and terminal oxygen atom (one that is attached only to the vanadium atom) and displacement of the water molecule from the special position. The final composition was found to be $Li_{0.3}V_{1.67}O_{3.67}\cdot H_2O$ with about 1/6 of the vanadium sites being vacant. The position of the lithium atom was not found even from neutron data due to its small amount and weak scattering. It is assumably located in the place of vacant vanadium atom or nearby.

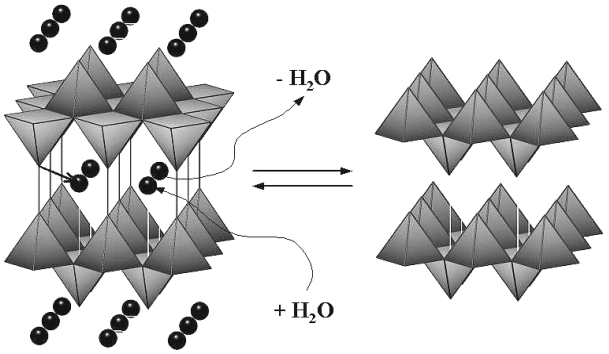

Fig. 7. Transformation between hydrated and anhydrous forms of $Li_xV_{2-\delta}O_{4-\delta}$.

This structure, constructed of vanadium square pyramids directed up and down in the chess-order (Figure 7), can be considered as the parent for many other vanadium oxide layers. Later, the same structure was found for another vanadium oxide (without lithium) using single crystal data [39].

$Li_xV_{2-\delta}O_{4-\delta}$ [40]

The anhydrous lithium vanadium oxide (sp. gr. P4/nmm, V=92.34(3) Å^3) forms when the hydrate is heated above 120°C. Its structure can be easily deducted from the hydrate as shown in Figure 7 assuming that apical oxygen atoms of the framework will slide into position from where water is removed. The Rietveld refinement confirmed this model.

4.3. Layered Vanadium Oxide Structures

Intercalation of the inorganic and organic ions between the vanadium oxide layers often increases the framework stability and the size and properties of the ions defines the type of the framework formed. Sometimes the ion size and the periodicity of the oxide framework are incommensurate, which yields disorder of ions or modulation of the framework that provides additional challenges for the structure determination especially from the powder data. However, the greatest challenge is relatively low vanadium scattering factor. This requires better accuracy of the initial model than for example in case of stronger scattering molybdenum. Thus, usually it is not enough to determine position of only vanadium atoms and therefore more advanced and powerful methods of the structure solution are needed.

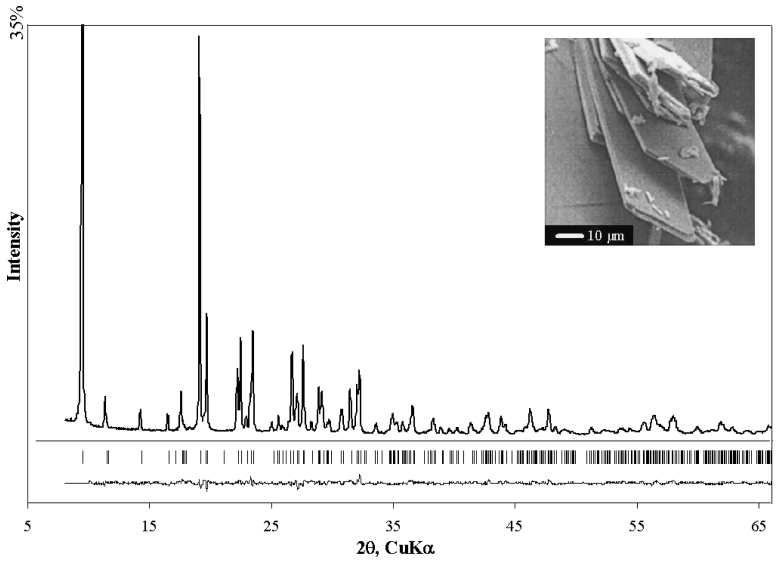

Fig. 8. The Rietveld refinement of $tmaV_3O_7$. Inset shows plate-like morphology of the crystals.

$tmaV_3O_7$ [41]

The powder pattern of this vanadate was indexed using ITO program in a primitive monoclinic lattice. However, its crystal structure was solved using direct methods only after the crystal-chemistry of the vanadium oxides (possible connectivity, polyhedra, etc.) was studied. Successful initial model contained three vanadium atoms and four of seven oxygen atoms. Rest of the oxygen atoms and five atoms of the organic ion were located from several sequential difference Fourier syntheses. The final Rietveld refinement (sp. gr. $P2_1/n$, $V=1020.1(1)$ Å^3, $2\theta_{max}=67°$, 424 reflections, 15 atoms, $R_B=5.2\%$, $R_p=7.8\%$, PO: WinCSD, axis 100, magnitude 2.7) revealed quite strong PO which could be expected from such thin plate-like crystals shown on the inset in Figure 8.

Resulting new type of the V_3O_7 layer appeared to be missing member of V_6O_{14} series [42], which along with quite reasonable bond lengths and polyhedra, confirms the correctness of the structure.

$tmaV_8O_{20}$ [8]

This thetramethylammonium vanadate was obtained at much lower pH than previous in form of only micron thick fibers (Figure 4,c). The diffraction peaks were quite broad ranging from 0.15 to 0.20° 2θ at low and medium angles. The peak shape was also unusual practically approaching pure Lorenzian that along with the elevated peak-width could be expected from the small size of the crystalline fibers. Indexing of this powder pattern succeeded only after excluding several weak low-angle peaks, which were assumably modulation satellites or impurity peaks.

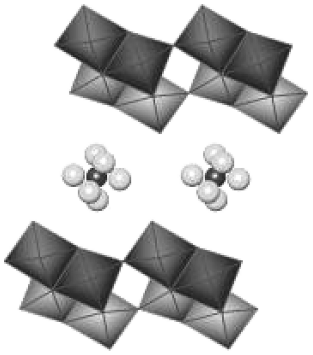

Fig. 9. The crystal structure of $tmaV_8O_{20}$: the vanadium oxide layer is shown with polyhedra and disordered the tma molecule with balls.

The structure solution was performed by direct methods using extracted integrated intensity yielding vanadium and some of the oxygen atoms. Rest of the oxygen atoms and atoms of the disordered organic ion were located from the difference Fourier maps. The final Rietveld refinement (sp. gr. C2/m, $V=523.1(1)$ Å^3, $R_B=6.71\%$, $R_p=6.77\%$, PO: March–Dollase, axis 100, magnitude 1.2) resulted reasonable structure with novel type of the layer that is made of quadruple octahedral chains sharing two corners as shown in Figure 9. This building block is found in other double-sheet vanadium oxide layers of different configuration. Disorder of the intercalated ion could be anticipated because of incompatibility between the ion size of about 6 Å and the repeat distance along the b axis that is only 3.6 Å. This type of

disorder happens quite often in the intercalated structures and was approximately modeled by occupationally disordered carbon and nitrogen atoms.

$tea V_8O_{20}$ and $imd_4V_8O_{20}$ [43]

Recently, two new compounds with the same type of the layer were prepared: tetraethylammonium (tea) and imidazolium (imd) vanadates. The first structure was solved using direct methods and is isostructural to $tmaV_8O_{20}$. It has similar morphology and gives similar powder pattern. The second material behaves differently. It has higher ion to metal ratio, crystallizes in a different space group ($P2_1/m$) with different cell dimensions, and forms very long and thin fibers, so thin that the sample looks like cotton. It cannot be packed and turns into the paste on grinding. The preferred orientation is very high and only few weak peaks that do not belong to *hk0* zone can be observed. This makes both the indexing and the structure solution quite difficult. Nevertheless, it was possible to solve the structure using FOX program. Optimized were two vanadium octahedra and imd molecule. The Rietveld refinement of the obtained model was performed using restrains on the imd geometry and some vanadium to oxygen distances. Interestingly, this structure appeared to be ordered, while the tea structure has the intercalated ion disordered similarly to and because of the same reason as $tmaV_8O_{20}$.

Vanadium oxide δ-phases

One of the most common vanadium oxide frameworks is so-called δ-phase that consists of a double sheet layer (Figure 10). This type of layers is made of the same quadruple chain of vanadium octahedra as the V_8O_{20} layer but the chains are linked by sharing edges. The repeat distance along the chain is about 3.7 Å, which often does not match larger intercalated species yielding disorder. Thus, the smaller ions such as metal ions, water, and ammonium are usually ordered as shown in Figure 10, while the larger molecules are not, such as, for example, methylammonium (ma), tetramethyl ammonium (tma), tetraethylammonium (tea), metal complexes, and others.

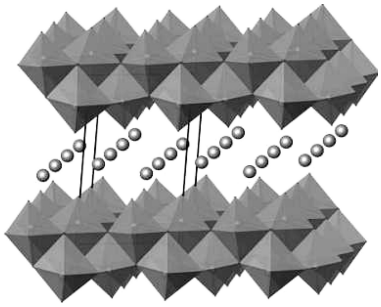

Fig. 10. Polyhedral representation of the δ-layer with ordered distribution of intercalated small ions.

The δ-phase usually form polycrystalline materials with plate-like or fiber-like morphology of the particles, which size often lies in the sub-micron range. This introduces a range of problems (typical for layered intercalates) in the indexing of the powder pattern, solving the structure and also the Rietveld refinement. These are broadening of the diffraction peaks (often anisotropic), strong preferred orientation, disorder, and others.

In most cases δ-phase crystallizes in a monoclinic system and space group C2/m. Sometimes intercalated species yield different stacking of the layers with higher or lower symmetry. In such cases the crystal structure has to be solved *ab initio* as was done for triclinic $Li_xtea_yV_4O_{10}\cdot nH_2O$ using synchrotron data [44]. Otherwise, when similar structure is identified, the δ-layer can be used as an initial structure model ($NH_4V_4O_{10}$ [44], $ma_xV_4O_{10}\cdot nH_2O$ [45], $tma_xM_yV_4O_{10}\cdot nH_2O$ (M=Fe, Zn, Mn) [46]). The intercalated ions are then located from the difference Fourier map. Only one of these four structures, $NH_4V_4O_{10}$, shows ordered distribution of the interlayer ions.

4.4. Mixed Transition Metals Frameworks

The layered battery materials show good cycling behavior but often their capacity retention is not so good. The layers may collapse when fully charged (all Li removed) or irreversibly transforms into another phase when overdischarged (too much Li inserted). The former case is found in commercial $LiCoO_2$ batteries, which can be destroyed when more than half Li atoms are removed. Many attempts are made to stabilize such layered materials. For example, it was found that intercalated species such as potassium in K_xMnO_2 [47] and tetramethyl ammonium in $tma_4[Zn_4V_{21}O_{58}]$ [48] improve the cycling stability by keeping layers apart. Different way is stabilizing the open framework itself by adding another metal that may or may not be red-ox inert. The search for new mixed open structures yielded variety of novel compounds. These compounds are not necessary electrochemically active or have the open framework. Still their crystal structure was determined and correlated with the cycling behavior. The powder diffraction data were used for structural characterization of the following compounds:

$Mn_7(OH)_3(VO_4)_4$* [49], $NiMnO_2(OH)$ [45], γ-MnV_2O_5 [7], $Zn_2(OH)_3VO_3$* [48], $Al_2(OH)_3VO_4$ [50], $Zn_3(OH)_2V_2O_7 \cdot 2H_2O$ [51], and others. The structure determination of the first two materials was not routine and is discussed below.

$NiMnO_2(OH)$ [45]

This material exhibits powder diffraction of good quality. Its crystal structure has an interesting three-dimensional extended framework

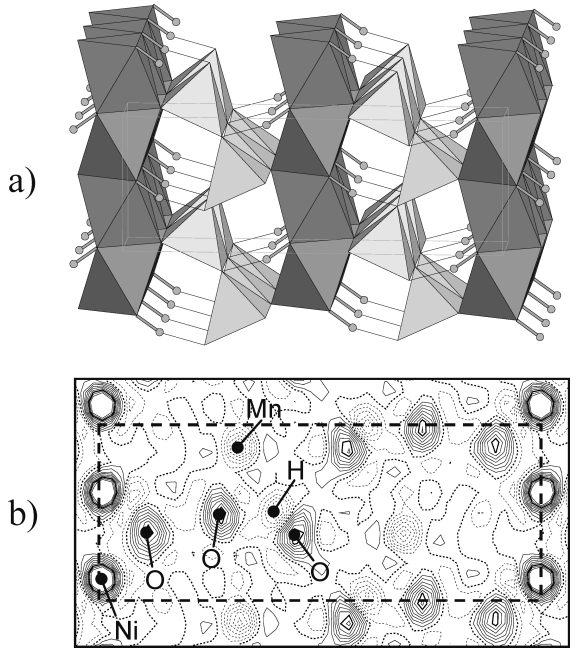

Fig. 11. Polyhedral representation of the $NiMnO_2$-(OH) (a) and the nuclear density distributions at $x=0$ (b). Solid lines show positive values, thin dotted lines negative, and thick dotted lines indicate zero level.

(Figure 11, a). Both powder pattern indexing and structure solution were habitual. However, the goal of the structure completion was to distinguish Ni and Mn atoms and to locate hydrogen atoms. The first was achieved by analysis of bond valence sum, which agreed with the electron density distribution. The hydrogen atoms were located from the difference Fourier map and then refined. The H atom forms typical hydrogen bond and therefore makes good chemical sense that is quite unusually for the powder method. Nonetheless, the neutron diffraction data were used as an additional confirmation, which is very reliable in this case because of the negative neutron scattering factor of the hydrogen and manganese atoms (Figure 11, b). The final Rietveld refinement was performed on combined X-ray and neutron data yielding low residual (sp. gr. $Cmc2_1$, $V=220.880(5)$ Å^3, $R_B=6.25\%$, $R_p=4.99\%$, PO: March–Dollase, axes 010 and 001, magnitude 3.99) and leaving no doubts in the distribution of the manganese and nickel atoms and location of the hydrogen atoms.

$Mn_7(OH)_3(VO_4)_4$ [49]

This material yields high quality powder data and has interesting pipe-like morphology (Figure 12). The composition $Mn_7(OH)_3(VO_4)_4$ assumes full occupation of all sites. However, structure refinement revealed occupational disorder for Mn atoms in the hexagonal tunnel and V and O atoms in the trigonal tunnel as marked in Figure 13 (top). The vacancy of the vanadium and oxygen atoms is in accord when vanadium

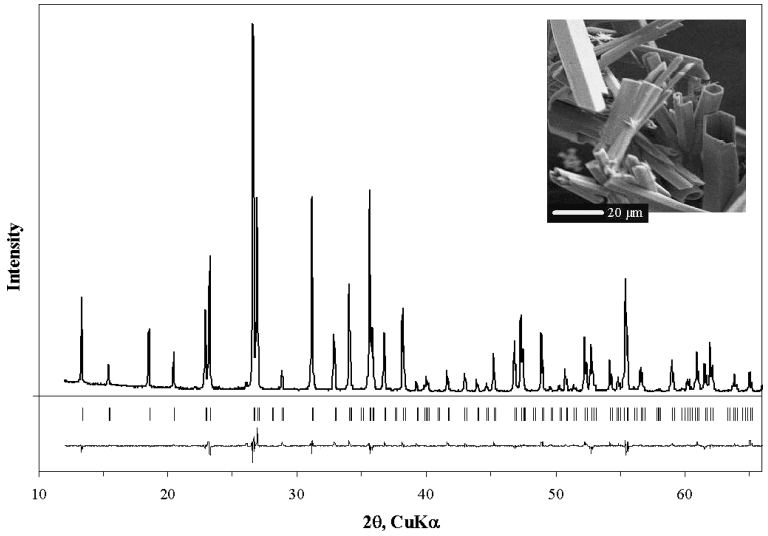

Fig. 12. The Rietveld plot of $Mn_7(OH)_3(VO_4)_4$. Inset shows pipe-like morphology of the crystals.

* Idealized composition.

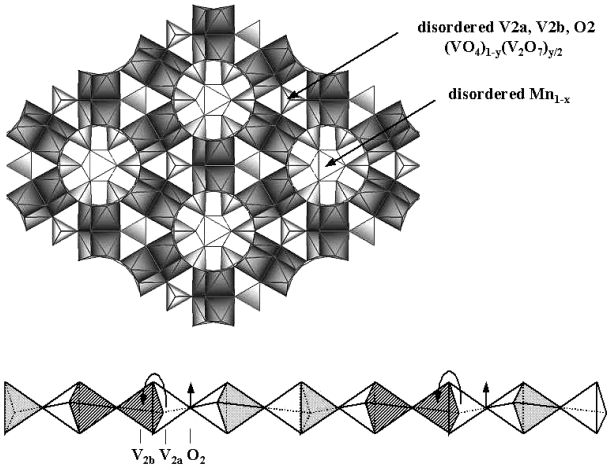

Fig. 13. Polyhedra representation of the $Mn_7(OH)_3(VO_4)_4$ structure (top) and VO_4–V_2O_7 disorder in the tunnel (bottom).

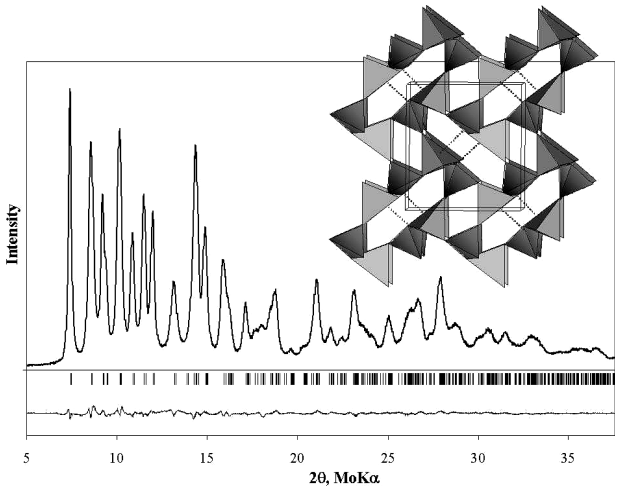

Fig. 14. The Rietveld plot and polyhedral representation of the monoclinic $FePO_4$.

tetrahedra flip as shown in Figure 13 (bottom). This yields the formation of divanadate group V_2O_7 and the following composition:

$$Mn_{7-x}(OH)_3(VO_4)_{4-y}(V_2O_7)_{y/2},$$

where x=0.137(4), y=0.195(4).

The final Rietveld refinement (sp. gr. $P6_3mc$, V=796.44(2) Å^3, $2\theta_{max}$=132°, 297 reflections, 10 atoms, R_B=8.7%, R_p=8.5%, PO: March–Dollase, axis 001, magnitude 2.7) yields good residuals. Recently, the disorder of the Mn, V and O atoms were confirmed* by single crystal data.†

4.5. Transition Metal Phosphates

Introduction of the phosphate group into the framework increases its stability during the cycling as well as the potential but for the cost of slightly lower capacity. Thus, phosphates of 3d transition metals are intensively explored for the battery applications. Here are discussed powder structure determination of novel iron phosphate, monoclinic $FePO_4$, and structural transformation of vanadyl phosphate through lithium intercalation/deintercalation process.

Monoclinic $FePO_4$ [52]

This compound forms as low crystallinity powder on the thermal decomposition of hydrated iron phosphate. The powder pattern, despite its low resolution (Figure 14), was successfully (but not routinely) used for the indexing and solving the structure as is detailed in [52].

The structure determination was performed using geometry optimization and energy minimization methods applied to the structural model, which was deducted using the knowledge of structural transformation of the hydrated orthorhombic iron phosphate into the anhydrous form. The final Rietveld refinement was conducted with restrained geometry of the PO_4 group yielding low residuals (sp. gr. $P2_1/n$, V=328.51(6) Å^3, $2\theta_{max}$=38°, 255 reflections, 6 atoms, R_B=3.2%, R_p=5.2%, PO: March–Dollase, axis 010, magnitude 1.5) and trigonal pyramidal coordination of the Fe atom. This framework is very similar to that found in iron arsenate (except slightly different distribution of short and long bonds in the Fe polyhedra), which is an additional confirmation of this structure correctness.

$VOPO_4$ and Its Li Derivatives [31]

The use of vanadyl phosphates as cathode material is promising because of their potentially high capacity, which is due to the wide range of the V oxidation states. The powder structure determination was intensively used for: structural characterization of the electrochemically intercalated materials, e.g. α-$LiVOPO_4$, structure determination including lithium distribution (ε-$VOPO_4$ and α-$Li_{1+x}VOPO_4$, x=0, 0.75), determination of the composition of the disordered phases (tetragonal $(VO)_xH_yPO_4$). This structural information explains transformation between the phases (Figure 15) and some structure–property relationships.

4.6. Electrolyte Salts and Related Compounds

In attempt to replace fluorine or arsenic containing lithium salts, which are currently in use as a source of conducting lithium ions in the

* P. Y. Zavalij: unpublished data.

† Bruker SmartApex diffractometer, 110 K, crystal size 0.10×0.02×0.007 mm, sp. gr. $P6_3mc$, a=13.2220(7) Å, c=5.2444(4) Å, V=794.00(8) Å^3, Rw=4.36%, R1=2.29%.

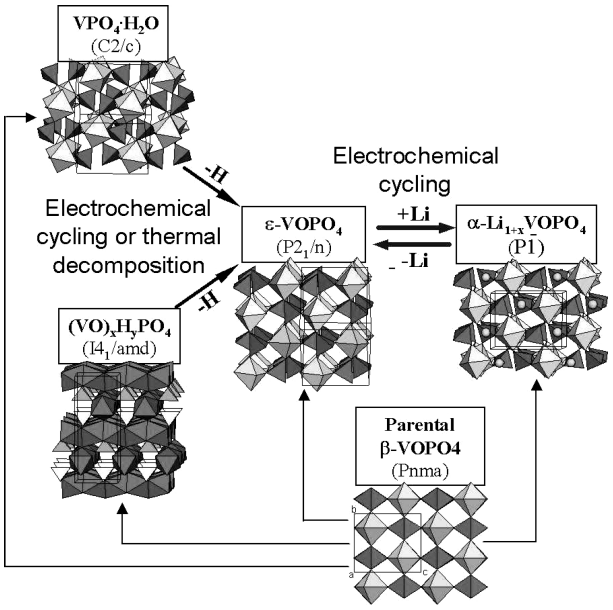

Fig. 15. The relationship between vanadyl phosphates and their lithium intercalates.

battery electrolytes, the new safer lithium bis(oxalato)borate (BOB) is being explored. However, its structure as well as structure of any other BOB compounds were unknown. Here, *ab initio* crystal structure determination from the powder data of Li, Na and K BOB salts is discussed.

$LiB(C_2O_4)_2$ [53]

This compound crystallizes in a form of fine white powder yielding relatively broad diffraction peaks (Figure 16). Multiple attempts to grow single crystal using variety of solvents yield only solvated crystals. Therefore, the powder structure determination was unavoidable. The challenge was not the fact that oxygen atoms were the heaviest in this compound but an accidental pseudo-hexagonal relationship between the cell dimensions of an orthorhombic cell. As result, the best indexing solution was always incorrect hexagonal cell but not the orthorhombic. This also imposes additional difficulties for structure solution since most of the diffraction peaks contain overlapped reflections. Thus, real space method of structure solution was a must. This was done by optimizing two species, Li atom and rigid body BOB molecule, using parallel tempering method realized in FOX software. Details on the indexing and solving the structure can be found in [53].

The final Rietveld refinement included restrains on the distances (but not the angles) of BOB and converged with low residuals (sp. gr. Pnma, V=636.99(6) Å^3, $2\theta_{max}$=60°, 104 reflections, 14 atoms, R_B=3.4%, R_p=9.4%, PO: spherical harmonics, magnitude 1.2) and reasonable square pyramidal environment of the Li atom.

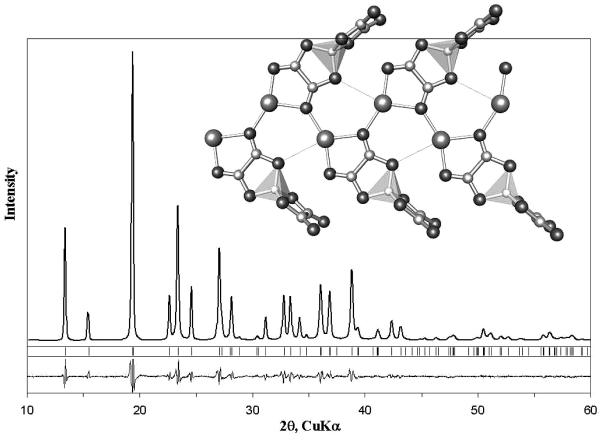

Fig. 16. The Rietveld plot and the crystal structure of $LiB(C_2O_4)_2$. Boron atoms are embraced with semi-transparent tetrahedra.

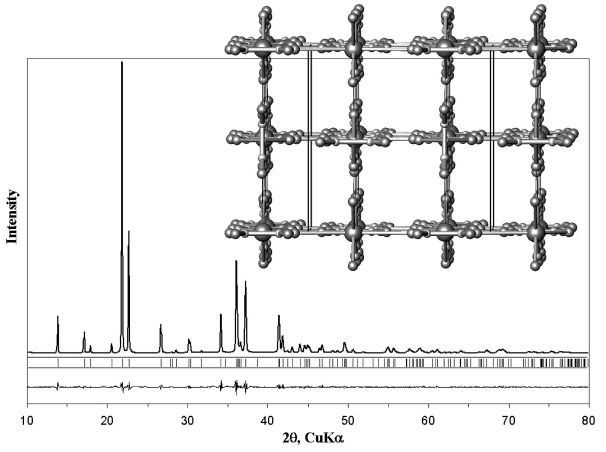

Fig. 17. The Rietveld plot and crystal structure of $NaB(C_2O_4)_2$.

M$B(C_2O_4)_2$ (*M*=Na, K) [53]

In order to gather more information about unknown structures of the BOB salts, corresponding sodium and potassium compounds were obtained and their crystal structure was determined from the powder diffraction data. Both materials appears to be highly crystalline and isostructural. The crystal structure of the potassium compound was solved by direct methods. The Rietveld refinement resulted very low residuals for both compounds (e.g. NaBOB: sp. gr. Cmcm, V=657.27(2) Å^3, $2\theta_{max}$=90°, 138 reflections, 14 atoms, R_B=3.1%, R_p=6.9%, PO: spherical harmonics, magnitude 1.4) and an interesting structure with square tunnels as shown in Figure 17.

Acknowledgement

This work was supported by the National Science Foundation through grant DMR-0313963.

References

[1] G. Ferey and A. K. Cheetham: Science, **283** (1999), 1125.
[2] S. Yang, P. Y. Zavalij, amd M. S. Whittingham: Electrochem. Commun., **5** (2003), 587.
[3] H. Bjork, S. Lidin, T. Gustafsson, and J. O. Thomas: Acta Cryst., **B57** (2001), 759.
[4] O. Bergstrom, T. Gustafsson, and J. O. Thomas: Acta Cryst., **C53** (1997), 528.
[5] O. Bergstrom, T. Gustafsson, and J. O. Thomas: Acta Cryst., **C54** (1998), 1204.
[6] C. Weeks, Y. Song, M. Suzuki, N. A. Chernova, P. Y. Zavalij, and M. S. Whittingham: J. Mater. Chem., **13** (2003), 1420.
[7] F. Zhang, P. Y. Zavalij, and M. S. Whittingham: Electrochem. Commun., (1999), 564.
[8] T. Chirayil, P. Y. Zavalij, and M. S. Whittingham: J. Mater. Chem., **7** (1997), 2193.
[9] J. W. Visser: J. Appl. Cryst., **2** (1969), 89.
[10] P.-E. Werner, L. Eriksson and M. Westdahl: J. Appl. Cryst., **18** (1985), 367.
[11] A. Boutlif and D. Louër: J. Appl. Cryst., **24** (1991), 987.
[12] A. Le Bail: McMaille, version 3, http://www.cristal.org/McMaille/ (2003).
[13] Materials Studio, Accelrys Inc., San Diego, CA, (2001).
[14] G. S. Pawley: J. Appl. Cryst., **14** (1981), 357.
[15] A. Le Bail, H. Duroy and J. L. Fourquet: Mat. Res. Bull., **23** (1988), 447.
[16] G. M. Sheldrick: Acta Cryst., **A46** (1990), 467.
[17] V. Favre-Nicolin and R. J. Cerny: J. Appl. Cryst., **35** (2002), 734.
[18] H. M. Rietveld: J. Appl. Cryst., **2** (1969), 65.
[19] W. A. Dollase: J. Appl. Cryst., **19** (1986), 267.
[20] R. B. Von Dreele: J. Appl. Cryst., **30** (1997), 517.
[21] A. C. Larson and R. B. Von Dreele: General Structure Analysis System (GSAS), Los Alamos National Laboratory Report LAUR 86-748, (2000).
[22] B. Hunter: Rietica—A visual Rietveld program, IUCr Commission on Powder Diffraction Newsletter No. 20, (1998).
[23] J. Rodriguez-Carvajal: FULLPROF: "A Program for Rietveld Refinement and Pattern Matching Analysis", Abstracts of the Satellite Meeting on Powder Diffraction of the XV Congress of the IUCr, Toulouse, France, (1990), 127.
[24] L. G. Akselrud, P. Y. Zavaliij, Yu. N. Grin, V. K. Pecharsky, B. Baumgartner, and E. Wolfel: Materials Science Forum, **133-136** (1993), 335.
[25] R. Jenkins, R. L. Snyder: Introduction to X-Ray Powder Diffractometry, Wiley-Interscience, (1996), 432.
[26] The Rietveld Method (International Union of Crystallography Monographs on Crystallography 5): ed. by R. A. Young, Oxford University Press, (1995), 312.
[27] Structure Determination from Powder Diffraction Data, ed. by W. I. F. David, K. Shankland, L. B. McCusker, Ch. Baerlocher, Oxford Press, (2002), 224.
[28] V. K. Pecharsky and P. Y. Zavalij: Fundamentals of Powder Diffraction and Structural Characterization of Materials, Kluwer Academic Publishers, (2003), 713.
[29] M. S. Whittingham: Electrochem. Soc. Proc., **99-24** (2000), 7.
[30] P. Y. Zavalij and M. S. Whittingham: Acta Cryst., **B55** (1999), 627.
[31] Y. Song, P. Y. Zavalij, and M. S. Whittingham: Inorg. Chem., (2003), in preparation.
[32] T. G. Chirayil, E. A. Boylan, M. Mamak, P. Y. Zavalij, and M. S. Whittingham: Chem. Comm., (1997), 33.
[33] T. Chirayil, P. Y. Zavalij, and M. S. Whittingham: Chem. Mater., **10** (1998), 2629.
[34] J.-D. Guo, P. Y. Zavalij, and M. S. Whittingham: Chem. Mater., **6** (1994), 357.
[35] N. Guillou, G. Ferey, and M. S. Whittingham: J. Mater. Chem., **8** (1998), 2277.
[36] P. Y. Zavalij and M. S. Whittingham: Acta Cryst., **C53** (1997), 1374.
[37] P. Tolédano, M. Touboul, and H. Paulette: Acta Cryst., **B32** (1976), 1859.
[38] T. Chirayil, P. Y. Zavalij., M. S. Whittingham: Solid State Ionics, **84** (1996), 163.
[39] D. Hagrman, J. Zubieta, C. J. Warren, L. M. Meyer, M. M. J. Treacy, and R. C. Haushalter: J. Solid State Chem., **138** (1998), 178.
[40] T. Chirayil, P. Y. Zavalij., M. S. Whittingham: J. Electrochem. Soc., **143** (1996), L193.
[41] P. Y. Zavalij, T. Chirayil, and M. S. Whittingham: Acta Cryst., **C53** (1997), 879.
[42] P. Y. Zavalij, F. Zhang, and M. S. Whittingham: Acta Cryst., **B55** (1999), 953.
[43] S. Lutta, C. Chen, N. Chernova, P. Y. Zavalij, and M. S. Whittingham: (2003), in preparation.
[44] S. Luta, Y. Song, N. Chernova, C. Botez, P. Stephens, P. Y. Zavalij, and M. S. Whittingham: (2003), in preparation.
[45] R. Chen, P. Y. Zavalij, M. S. Whittingham, J. E. Greedan, N. P. Raju, and M. Bieringer: J. Mater. Chem., **9** (1999), 93.
[46] J. K. Ngala, P. Y. Zavalij, and M. S. Whittingham: Mater. Res. Soc. Proc., **658** (2001) GG9.16.1.
[47] R. Chen, P. Zavalij, M. S. Whittingham: Chem. Mater., **8** (1996), 1275.
[48] P. Y. Zavalij, F. Zhang, and M. S. Whittingham: Solid State Sciences, **4** (2002), 591.
[49] F. Zhang, P. Y. Zavalij, and M. S. Whittingham: J. Mater. Chem., **9** (1999), 3137.
[50] B. Pecquenard, P. Y. Zavalij, and M. Stanley Whittingham: J. Mater. Chem., (1998) 1255.
[51] P. Y. Zavalij, F. Zhang, and M. S. Whittingham: Acta Cryst., **C53** (1997), 1738.
[52] Y. Song, P. Y. Zavalij, M. Suzuki, and M. S. Whittingham: Inorg. Chem., **41** (2002), 5778.
[53] P. Y. Zavalij, S. Yang, and M. S. Whittingham: Acta Cryst., **B59** (2003), 753.